J|A|C|S
ARTICLES

Published on Web 02/18/2009

SiC(0001) 3 × 3 Heterochirality Revealed by Single-Molecule STM Imaging

Guillaume Baffou,*,[†] Andrew J. Mayne,[†] Geneviève Comtet,[†] Gérald Dujardin,[†]
Louise Stauffer,[‡] and Philippe Sonnet[‡]

Laboratoire de Photophysique Moléculaire, Université Paris XI, 91405 Orsay, France, and Institut de Science des Matériaux de Mulhouse (IS2M), LRC CNRS 7228, Université de Haute Alsace, 68093 Mulhouse, France

Received July 31, 2008; E-mail: guillaume.baffou@u-psud.fr

Abstract: We report a description of the SiC(0001) 3 × 3 silicon carbide reconstruction based on single-molecule scanning tunneling microscopy (STM) observations and density functional theory calculations. We show that the SiC(0001) 3 × 3 reconstruction can be described as contiguous domains of right and left chirality distributed at the nanoscale, which breaks the to date supposed translational invariance of the surface. While this surface heterochirality remains invisible in STM topographies of clean surfaces, individual metal-free phthalocyanine molecules chemisorbed on the surface act as molecular lenses to reveal the surface chirality in the STM topographies. This original method exemplifies the ability of STM to probe atomic-scale structures in detail and provides a more complete vision of a frequently studied SiC reconstruction.

Introduction

Pasteur's introduction of the concept of molecular chirality in 1848 generated a revolution within science.[1] Now, over 150 years later, chiral surfaces capable of existing in two distinguishable mirror forms that cannot be superimposed are becoming important aspects of modern surface science, driven by the demand for heterogeneous asymmetrical catalysis and enantioselective molecule selection.[2−9] The recent success in the study of chiral surfaces at the molecular level has been enriched with the maturity of surface-science techniques such as scanning tunneling microscopy (STM),[3−5,10] low-energy electronic diffraction (LEED),[11] X-ray diffraction (XRD),[12] nonlinear optical techniques,[13] and density functional theory (DFT) calculations.[14]

Silicon carbide (SiC), like diamond and noble metals, is one of the rare biocompatible materials that, by means of organic functionalization of suitably selected SiC surfaces, could lead to the creation of hybrid organic−inorganic materials as the basis of new biosensors implantable in vivo.[15,16] In addition to having a large variety of polytypes, which enables the bulk band gap to be tuned from 2.4 to 3.2 eV, SiC offers a large choice of surface reconstructions.[17−21] The SiC(0001) 3 × 3 reconstruction in particular has received much attention. This Si-rich reconstruction is generated by silicon deposition. Interestingly, the generally accepted crystallographic model of the SiC(0001) 3 × 3 reconstruction[22] is based on a chiral unit cell. However, no evidence of chirality has yet been provided by any experimental surface-science technique.

In this paper, we show how single-phthalocyanine-molecule STM imaging can reveal the surface chirality underneath each molecule and thereby provide a more precise description of the SiC(0001) 3 × 3 reconstruction. Multiple molecular topographies indicate that the SiC(0001) 3 × 3 reconstruction could

---

[†] Université Paris XI.
[‡] Université de Haute Alsace.

(1) Prelog, V. *Science* **1976**, *193*, 17.
(2) Hazen, R. M.; Sholl, D. S. *Nat. Mater.* **2003**, *2*, 367.
(3) Lorenzo, M. O.; Baddeley, C. J.; Muryn, C.; Raval, R. *Nature* **2000**, *404*, 376.
(4) Kühnle, A.; Linderoth, T. R.; Besenbacher, F. *J. Am. Chem. Soc.* **2006**, *128*, 1076.
(5) Yamada, Y.; Girard, A.; Asaoka, H.; Yamamoto, H.; Shamoto, S. *Phys. Rev. B* **2008**, *77*, 153305.
(6) Chena, Q.; Richardson, N. V. *Annu. Rep. Prog. Chem.* **2004**, *100*, 313.
(7) Mallat, T.; Orglmeister, E.; Baiker, A. *Chem. Rev.* **2007**, *107*, 4863.
(8) Horvath, J. D.; Koritnik, A.; Kamakoti, P.; Sholl, D. S.; Gellman, A. J. *J. Am. Chem. Soc.* **2004**, *126*, 14988.
(9) Gladys, M. J.; Stevens, A. V.; Scott, N. R.; Jones, G.; Batchelor, D.; Held, G. *J. Phys. Chem. C* **2007**, *111*, 8331.
(10) Kühnle, A.; Linderoth, T. R.; Hammer, B.; Besenbacher, F. *Nature* **2002**, *415*, 891.
(11) Parschau, M.; Romer, S.; Ernst, K. H. *J. Am. Chem. Soc.* **2004**, *126*, 15398.
(12) Widmer, R.; Haug, F. J.; Ruffieux, P.; Gröning, O.; Bielmann, M.; Gröning, P.; Fasel, R. *J. Am. Chem. Soc.* **2006**, *128*, 14103.
(13) Verbiest, T.; Kauranen, M.; Maki, J. J.; Teerenstra, M. N.; Schouten, A. J.; Nolte, R. J. M.; Persoons, A. *J. Chem. Phys.* **1995**, *102*, 8296.
(14) Mae, K.; Morikawa, Y. *Surf. Sci.* **2004**, *553*, L63.
(15) Härtl, A.; Schmich, E.; Garrido, J. A.; Hernando, J.; Catharino, S. C. R.; Walter, S.; Feulner, P.; Kromka, A.; Steinmüller, D.; Stutzmann, M. *Nat. Mater.* **2004**, *3*, 736.
(16) Baffou, G.; Mayne, A. J.; Comtet, G.; Dujardin, G.; Sonnet, P.; Stauffer, L. *Appl. Phys. Lett.* **2007**, *91*, 073101.
(17) Starke, U.; Tallarida, M.; Kumar, A.; Horn, K.; Seifarth, O.; Kipp, L. *Mater. Sci. Forum* **2004**, *457−460*, 391.
(18) Li, L.; Tsong, I. S. T. *Surf. Sci.* **1996**, *351*, 141.
(19) Soukiassian, P.; Semond, F.; Douillard, L.; Mayne, A.; Dujardin, G.; Pizzagilli, L.; Joachim, C. *Phys. Rev. Lett.* **1997**, *78*, 907.
(20) Derycke, V.; Soukiassian, P.; Mayne, A.; Dujardin, G.; Gautier, J. *Phys. Rev. Lett.* **1998**, *81*, 5868.
(21) Amy, F.; Enriquez, H.; Soukiassian, P.; Storino, P.-F.; Chabal, Y. J.; Mayne, A. J.; Dujardin, G.; Hwu, Y. K.; Brylinski, C. *Phys. Rev. Lett.* **2001**, *86*, 4342.
(22) Schardt, J.; Bernhardt, J.; Starke, U.; Heinz, K. *Phys. Rev. B* **2000**, *62*, 10335.

10.1021/ja806002k CCC: $40.75

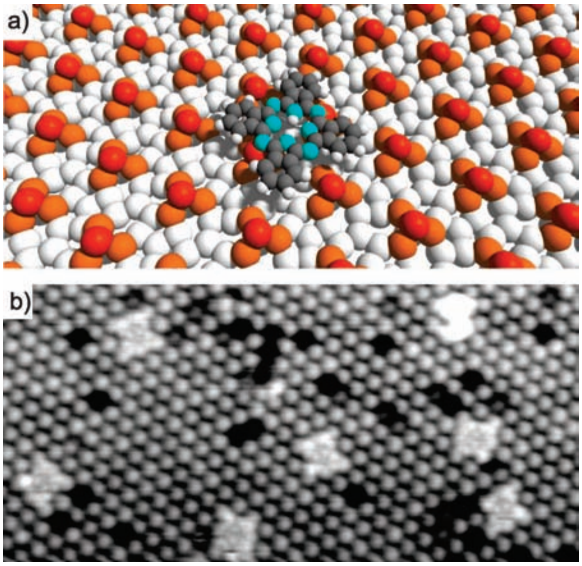

Figure 1. (a) 3D atomic structure of the phthalocyanine molecule (blue and gray atoms) adsorbed on the SiC(0001) 3 × 3 reconstruction, showing the silicon pyramid-like structures (red and orange atoms) lying on a silicon adlayer (white atoms). The molecule is chemisorbed onto two pyramids through two Si−N bonds formed via a [10 + 2] cycloaddition. (b) STM topography of isolated H_2Pc molecules deposited on the SiC(0001) 3 × 3 surface (30 nm × 15 nm, $V = -2.5$ V, $I = 0.3$ nA).

be heterochiral, consisting of coexisting, contiguous domains of opposite chirality distributed at the nanoscale. Supporting DFT calculations give an estimation of the energy required to change the local chirality. The results indicate that this heterochiral surface model is energetically reasonable and provides better agreement with previous experimental XRD results.

Materials and Methods

Experiments were performed using a room-temperature ultrahigh vacuum (UHV) STM apparatus. In our setup, the voltage V refers to the sample. We used n-doped 6*H*-SiC(0001) single-crystal wafers provided by Cree Research. The SiC sample was outgassed for a few hours and then flashed several times to ∼1100 °C to remove the native oxide and other impurities. It was then annealed at 650 °C for a few minutes under a silicon flux. A further annealing at 740 °C led to a well-reconstructed 3 × 3 surface, as indicated by a sharp LEED pattern.[23] High-purity (99%) metal-free phthalocyanine (H_2Pc) molecules supplied by Aldrich were deposited on the SiC samples by sublimation under UHV. Prior to sublimation, the molecule powder was outgassed at a temperature slightly above the temperature used for deposition. During the exposure, the H_2Pc molecules were heated to ∼250 °C while the substrate was held at room temperature.

Results and Discussion

Molecular Topographies. Figure 1a is a three-dimensional (3D) representation of the atomic structure of a H_2Pc molecule chemisorbed on the SiC(0001) 3 × 3 reconstruction. Only the top three silicon layers of the surface have been represented; for clarity, the Si−C layers of the bulk underneath the reconstruction are not shown. The SiC(0001) 3 × 3 reconstruction consists of a dense silicon adlayer (white) supporting silicon trimers (orange) with an adatom on top (red). The dangling bonds (DBs) of this reconstruction are specifically located on top of the pyramids. This pyramid-like model was proposed by Schardt et al.[22] and is the model that best matches experiment. The pyramid structures are separated by 9.24 Å, which confers an exceptionally low density of dangling bonds, unique chemical properties,[16] and strong electronic correlation properties.[24] In the STM image (Figure 1b), the surface is seen as a hexagonal array of small protrusions (corresponding to the adatoms of the pyramids of the 3 × 3 reconstruction) with a number of dark defects (missing protrusions). The STM image also shows six isolated H_2Pc molecules for a typical molecule coverage (0.05 monolayer). Each phthalocyanine molecule has a square shape with a distinct internal structure. In a recent study,[16] we showed that the H_2Pc molecules are chemisorbed on the surface through two Si−N bonds to two pyramids of the surface. The silicon atoms involved are the top adatoms of the pyramid structures; the nitrogen atoms involved are on diametrically opposite sides of the H_2Pc molecule, and the N−N separation closely matches the distance between two neighboring pyramids of the surface structure. The molecule remains planar and shows a very slight distortion away from being square. This adsorption configuration is symmetrical, particularly stable, and energetically favorable. The adsorption mechanism can be partially assimilated to a [10 + 2] Diels−Alder cycloaddition. Because of the threefold symmetry of the surface, H_2Pc molecules can display three equivalent orientations. The molecular orientation can easily be determined by examining the orientation of the two small spots inside the molecule that are aligned along a pyramid row of the surface. These two small spots are clearly visible in Figures 2 and 4.

At first sight, the molecular topographies all look very similar; in particular, they are systematically characterized by these clearly defined small spots in the center of each molecule. However, the high resolution of the STM image shows that the four corners of the molecule are not identical (Figure 2b). Each of the four molecular legs can appear in two different forms, which we shall name A and B. Some images with particularly high resolution (e.g., ABAB in Figure 2c) revealed that both A and B legs have three components, of which one is usually brighter (red or green spots) than the other two (blue spots), which are systematic and common to both types of leg. When the resolution does not allow these three spots to be distinguished separately, the global shape of the A and B legs is usually sufficient to identify their nature. Whenever a molecular configuration could not be straightforwardly determined from the topography, it was not included in the statistics. Surprisingly, A and B configurations seem to appear independently at each molecular leg, giving rise to 2^4 possible molecular configurations. However, among these 16 configurations, some are equivalent (degenerate) for symmetry reasons, leading to only *seven* different classes of equivalent configurations: (AAAA), (AAAB), (ABAB), (ABBA), (AABB), (ABBB), and (BBBB). A class of equivalent configurations is indicated by brackets, e.g., (ABAB) = {ABAB,BABA}. As Figure 2c shows, all of the classes were observed except for the (BBBB) class. The A and B legs seem to influence the molecular stability, which can be seen in the statistics. The configurations (ABBB), (AABB), and (BBBB) are observed less frequently than (AAAB) and (ABAB), indicating that having two contiguous B legs is energetically less favorable. See Explanation of the Multiple Topographies (below) for a discussion concerning the statistics.

---

(23) Amy, F.; Enriquez, H.; Soukiassian, P.; Brylinski, C.; Mayne, A.; Dujardin, G. *Appl. Phys. Lett.* **2001**, *79*, 767.

(24) Baffou, G.; Mayne, A. J.; Comtet, G.; Dujardin, G. *Phys. Rev. B* **2008**, *77*, 165320.

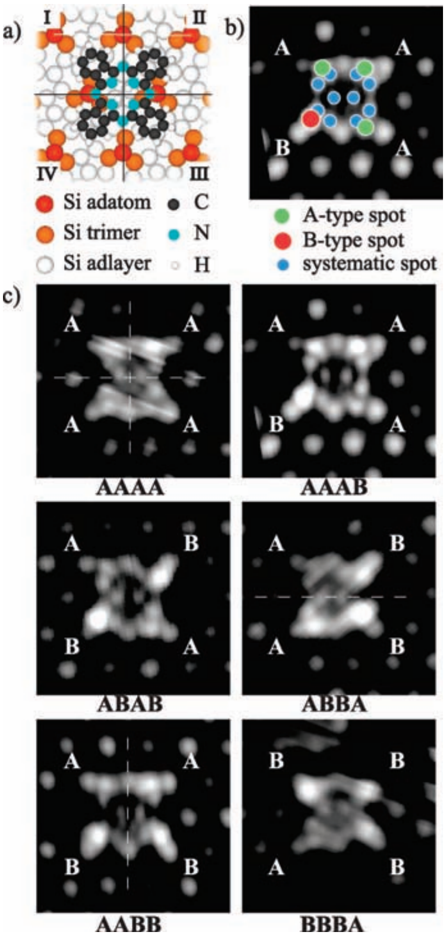

Figure 2. (a) Atomic structure of an H_2Pc molecule chemisorbed on the SiC(0001) 3 × 3 reconstruction (2.3 nm × 2.3 nm). The image is divided into four quadrants, each of which defines one of the four legs. (b) AAAB molecule with the internal detail of each leg highlighted. Each leg is composed of three spots, two systematic ones (blue) and a leg-specific one (green for A legs and red for B legs). (c) Multiple STM topographies of individual phthalocyanine molecules (4.4 nm × 4.4 nm). Average imaging parameters: $V = -2.3$ V, $I = 0.3$ nA. Each quadrant of the molecular topography can display one of two possible independent configurations (A or B), giving the different classes named (AAAA), (AAAB), (ABAB), (ABBA), (AABB), and (BBBA). Dashed lines represent symmetry axes where they exist.

In the literature, a number of STM experiments have reported multiple molecular STM topographies, on both metal[25−34] and semiconducting surfaces.[35−39] Among these results, two different situations are distinguishable that can give rise to multiple topographies: either the molecules are adsorbed on different, nonequivalent sites on the surface or the molecules are chemically modified, e.g., through cis−trans isomerizations or bond breaking within the molecule.[39] The multiple topographies reported here originate from the surface properties and not from the molecules themselves; indeed, only one type of adsorption site exists, and all of the adsorbed molecules are chemically identical. Occasional tip-induced motion of the H_2Pc molecules enabled us to reach this conclusion on the basis of the following observations: (i) without exception, if a molecule remained at the same surface site, it kept the same configuration regardless of the number of successive STM images and the duration of the experiment; (ii) if the molecule diffused from one site to another apparently *equivalent* site, the new conformation was very likely to be different; and (iii) if the molecule diffused on the surface and returned to its previous site, it recovered its original configuration. In addition to these three observations, the following remark should be considered: the four legs of the phthalocyanine are relatively rigid because they are an integral part of the π system, so we could expect no independent changes in the leg conformations. This is very different from other molecules such as lander molecules[40] or the Cu−TBPP molecule,[41] where partial rotation about a C−C single bond allows the legs to display a number of independent conformations. Furthermore, in contrast to the recent observation of different molecular configurations on an insulating surface,[42] which were considered to be induced by surface defects, in this case the influence of defects can be ruled out because both A and B legs can be observed on molecules that have no nearby defects. These points led us to propose that the nature of the molecular topography depends only on the *localization* of the molecule over the surface, despite the homogeneous appearance of the STM images of the bare surface. In other words, the H_2Pc molecules act as molecular revealers or "lenses" (in the sense that they can reveal something hidden) that probe the underlying surface reconstruction and reveal that the atomic conformations differ from one unit cell to another. This clearly calls into question the homogeneity of the SiC(0001) 3 × 3 reconstruction. While STM topographies themselves do not reveal the actual atomic structure of the underlying surface, we will show that the Starke reconstruction[22] can undergo possible local isomerizations that could explain both the number and the symmetry of the multiple molecular topographies.

Multiple Surface Conformations. Modifications of the Starke unit cell are considered only if they conserve the number of atoms, the tetravalence of all of the Si atoms, and reasonable interatomic distances. A proposed modification that could explain our results is presented in Figure 3. Figure 3a,b shows the transformation, using the unrelaxed atomic positions to simplify the explanation. In the unrelaxed atomic structure, all of the atoms are located on the nodes of a hexagonal lattice.

---

(25) Liljeroth, P.; Repp, J.; Meyer, G. *Science* **2007**, *317*, 1203.
(26) Qiu, X. H.; Nazin, G. V.; Ho, W. *Phys. Rev. Lett.* **2004**, *93*, 196806.
(27) Iancu, V.; Hla, S. W. *Proc. Natl. Acad. Sci. U.S.A.* **2006**, *103*, 13718.
(28) Alemani, M.; Peters, M. V.; Hecht, S.; Rieder, K.-H.; Moresco, F.; Grill, L. *J. Am. Chem. Soc.* **2006**, *128*, 14446.
(29) Choi, B. Y.; Kahng, S. J.; Kim, S.; Kim, H.; Kim, H. W.; Song, Y. J.; Ihm, J.; Kuk, Y. *Phys. Rev. Lett.* **2007**, *96*, 156106.
(30) Miwa, J. A.; Weigelt, S.; Gersen, H.; Besenbacher, F.; Rosei, F.; Linderoth, T. R. *J. Am. Chem. Soc.* **2006**, *128*, 3164.
(31) Tsai, C. S.; Wang, J. K.; Skodje, R. T.; Lin, J. C. *J. Am. Chem. Soc.* **2005**, *127*, 10788.
(32) Simic-Milosevic, S.; Mehlhorn, M.; Rieder, K.-H.; Meyer, J.; Morgenstern, K. *Phys. Rev. Lett.* **2007**, *98*, 116102.
(33) Henzl, J.; Mehlhorn, M.; Gawronski, H.; Rieder, K.-H.; Morgenstern, K. *Angew. Chem., Int. Ed.* **2006**, *45*, 603.
(34) Comstock, M. J.; Levy, N.; Kirakosian, A.; Cho, J.; Lauterwasser, F.; Harvey, J. H.; Strubbe, D. A.; Fréchet, J. M. J.; Trauner, D.; Louie, S. G.; Crommie, M. F. *Phys. Rev. Lett.* **2007**, *99*, 038301.
(35) Hofer, W. A.; Fisher, A. J.; Lopinski, G. P.; Wolkow, R. A. *Phys. Rev. B* **2001**, *63*, 085314.
(36) Bellec, A.; Cranney, M.; Chalopin, Y.; Mayne, A. J.; Comtet, G.; Dujardin, G. *J. Phys. Chem. C* **2007**, *111*, 14818.
(37) Soukiassian, L.; Mayne, A. J.; Comtet, G.; Hellner, L.; Dujardin, G.; Gourdon, A. *J. Chem. Phys.* **2005**, *122*, 134704.
(38) Mamatkulov, M.; Sonnet, P.; Stauffer, L.; Minot, C. *Phys. Rev. B* **2007**, *76*, 115333.
(39) Mamatkulov, M.; Stauffer, L.; Sonnet, P.; Mayne, A. J.; Comtet, G.; Dujardin, G. *J. Chem. Phys.* **2008**, *128*, 244710.
(40) Alemani, M.; Gross, L.; Moresco, F.; Rieder, K.-H.; Wang, C.; Bouju, X.; Gourdon, A.; Joachim, C. *Chem. Phys. Lett.* **2005**, *402*, 180.
(41) Moresco, F.; Meyer, G.; Rieder, K.-H.; Tang, H.; Gourdon, A.; Joachim, C. *Phys. Rev. Lett.* **2001**, *86*, 672.
(42) Qiu, X. H.; Nazin, G. V.; Ho, W. *Science* **2003**, *299*, 542.

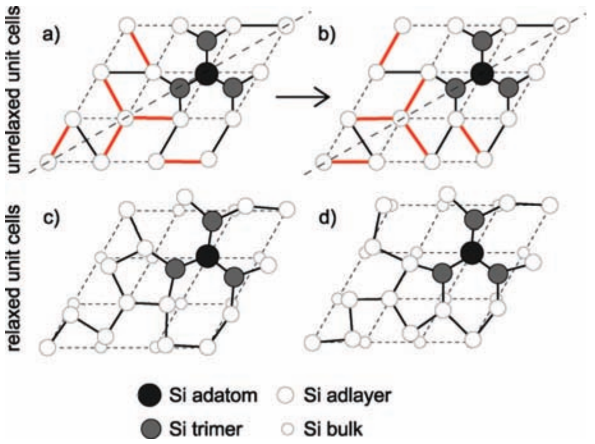

Figure 3. Atomic schematics explaining the possible isomerizations of the unit cells in the Starke reconstruction. (a) Unrelaxed Starke unit cell. (b) Modification of some chemical bonds, giving a unit cell with the opposite chirality. (c, d) Corresponding relaxed structures calculated with DFT simulations. The rhombus-like dotted lines represent the bulk 1 × 1 unit cell, and the transverse dashed lines in (a) and (b) represent the mirror axis of symmetry.

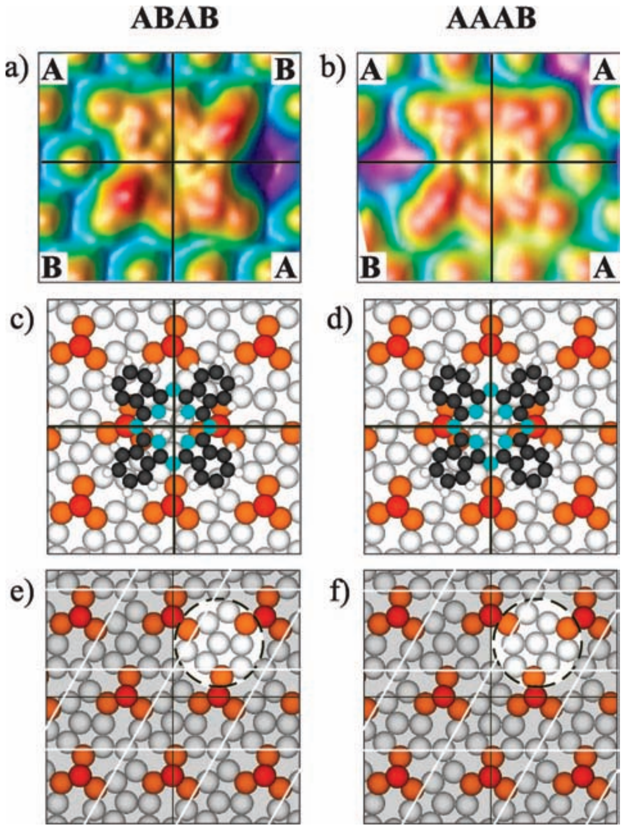

Figure 4. Local modification of the SiC(0001) 3 × 3 reconstruction underneath a molecular leg that can explain the multiple conformations. (a, b) STM topographies of two selected molecules, having (a) ABAB and (b) AAAB conformations. The only significant difference concerns the upper right corner. (c, d) Associated relaxed atomic structures with different surface structures, showing that the environment of each leg indeed corresponds to the respective ABAB and AAAB symmetries. (e, f) Pictures corresponding to (c) and (d) with the molecule removed to show the precise surface transformation (dashed circles). The unit cells are indicated to facilitate the comparison with Figure 3.

This transformation concerns six Si−Si chemical bonds (red) within the silicon adlayer of the reconstruction only. The important point is that the transformation can be performed locally, within a unique unit cell of the reconstruction, which is precisely what is required in order to allow the translationally invariant symmetry to be broken.

Further insight can be obtained by considering a fundamental feature of the Starke unit cell: it is noncentrosymmetric and chiral, which breaks the centrosymmetry of the 1 × 1 unreconstructed surface on which the 3 × 3 reconstruction is formed. This implies that during the formation of the 3 × 3 surface (i.e., during silicon deposition on the 1 × 1 reconstruction), two equivalent, degenerate, and equiprobable reconstructions can be formed, one with right and the other with left chirality. Here, the designations "right" and "left" are arbitrary, and we have chosen to attribute the name "right chirality" to the Starke unit cell represented in Figure 3a. Interestingly, the modified cell represented in Figure 3b turns out to have the opposite left chirality. By comparing panels a and b of Figure 3, we can see that the long axis of the rhombus-like unit cell is indeed a mirror axis of symmetry. Consequently, a consideration of the symmetry and bonding allows left- and right-handed unit cells to coexist *contiguously* on the same surface. To verify this proposition for the SiC(0001) 3 × 3 reconstruction and notably that the contiguity of unit cells of opposite chirality remains energetically favorable, numerical simulations were performed.

DFT Calculations. We performed DFT simulations by using the VASP code[43−45] to calculate the relaxed atomic structure and the energy change associated with a local change of the chirality. The generalized gradient approximation (GGA) and ultrasoft pseudopotentials[46,47] were employed. The SiC(0001) 3 × 3 surface was modeled as a periodic slab involving six layers (three layers for the reconstruction, one bilayer of SiC, and one layer of hydrogen atoms). H atoms were added on the back side to saturate the DBs. An investigation of the local modifications of the reconstruction required the use of a 9 × 9 supercell lattice (composed of nine 3 × 3 unit cells) in which only one 3 × 3 unit cell was modified with respect to Figure 3b. The size of the supercell ensured that the modified unit cells of the lattice were far enough apart to be considered as independent, allowing a reliable estimation of the energy change for a local transformation to be made.

The relaxed structure converged to a stable configuration. The Starke unit cell is displayed in Figure 3c and the modified unit cell of the 9 × 9 supercell in Figure 3d. In the modified configuration, all of the bond strengths are less than 50 meV/Å, which is the reference value usually employed in DFT calculations. We can thus conclude that the structure is favorable. The energy change for the modification turned out to be positive: +2.5 eV. This result shows that the more favorable situation is a homochiral reconstruction (whatever the chirality) and that the presence of contiguous opposite chiralities constitutes a metastable state of the SiC(0001) 3 × 3 reconstruction. A heterochiral reconstruction cannot relax to a homochiral ground state, since this would require a huge number of chemical bonds to be broken. Since right and left homochiral reconstructions should have the same energy, the higher energy of the heterochiral reconstruction originates from the *boundaries* that separate the right- and left-handed homochiral domains. We also performed simulations containing three contiguous modified unit cells. When only one unit cell was modified, the

---

(43) Kresse, G.; Hafner, J. *Phys. Rev. B* **1994**, *49*, 14251.
(44) Kresse, G.; Furthmüller, J. *Comput. Mater. Sci.* **1996**, *6*, 15.
(45) Kresse, G.; Furthmüller, J. *Phys. Rev. B* **1996**, *54*, 11169.
(46) Vanderbilt, D. *Phys. Rev. B* **1990**, *41*, 7892.
(47) Kresse, G.; Hafner, J. *J. Phys.: Condens. Matter* **1994**, *6*, 8245.

affected area was confined within an equilateral triangle, corresponding to the lower left corner of Figure 3c. When three contiguous unit cells were modified, the affected area was confined within an equilateral triangle having a perimeter twice as large and a surface area four times larger. The energy change for this modification was +5.0 eV, which is exactly twice that of a single modified unit cell. This confirms that the energy change arises from the boundaries between the domains of opposite chirality. We can therefore simply deduce that the energy change per unit length of the boundary is 90 meV/Å.

To reduce the number of boundaries and thus the energy change, it is likely that a SiC(0001) 3 × 3 reconstruction consists of left- and right-handed contiguous *domains* rather than randomly distributed isolated marginal unit cells. Experimentally, heterochirality is observed instead of a homochiral ground state, since the entropy of the system is increased markedly. Sample temperature, Si deposition rate, and exposure time are the three parameters that one could vary in order to achieve thermodynamic control leading to a homochiral reconstruction. Such a homochiral reconstruction would be a prerequisite for enantiospecific applications.

Explanation of the Multiple Topographies. We shall see that this description of the SiC(0001) 3 × 3 surface in terms of coexisting right- and left-handed domains can explain *both* the number and the symmetries of the molecular configuration classes. As an example, Figure 4 compares the configurations ABAB (left column) and AAAB (right column). High-resolution STM topographies and associated atomic structures are presented for both of these configurations. The left column corresponds to the homochiral Starke reconstruction: no cell has been modified. In looking carefully at Figure 4c, we notice that the Si adlayer underneath two diametrically opposed legs looks exactly the same (i.e., two opposite legs "see" the same local surface atomic structure) but that it looks different for two contiguous legs. As a consequence, a uniform chirality (left or right) is associated with an ABAB (or BABA) symmetry. In the right column of Figure 4, a local modification of the chirality of the adlayer was performed in quadrant II (quadrant numbers are defined in Figure 2a). Therefore, this new situation no longer corresponds to a homochiral reconstruction. Dashed circles have been added in Figure 4e,f to highlight this modification more clearly. First, a local modification of the chirality of the adlayer can occur precisely underneath a molecular leg. Then, as Figure 4d shows, the leg of the molecule in quadrant II has silicon adlayer atoms in relative positions similar to those in the neighboring quadrants I and III. Thus, we obtain an AAAB-like symmetry. Let us note that one might have expected the formation of a new type of leg, C, to give an ACAB configuration, but such is not the case. This new description of the SiC(0001) 3 × 3 reconstruction is thus well-suited for explaining in detail both the nature and the symmetries of the multiple topographies.

A direct piece of evidence for this description would have been calculations of the molecular topographies using a semiemprical model to retrieve the morphology of the STM topographies. However, modeling a large molecule on such a big unit cell is beyond the capability of this method. Furthermore, it is likely that the precise topography results from the molecular flip-flop motion around the two Si−N bonds induced by scanning of the tip across the molecule, which would make the topography even more complicated to decipher.

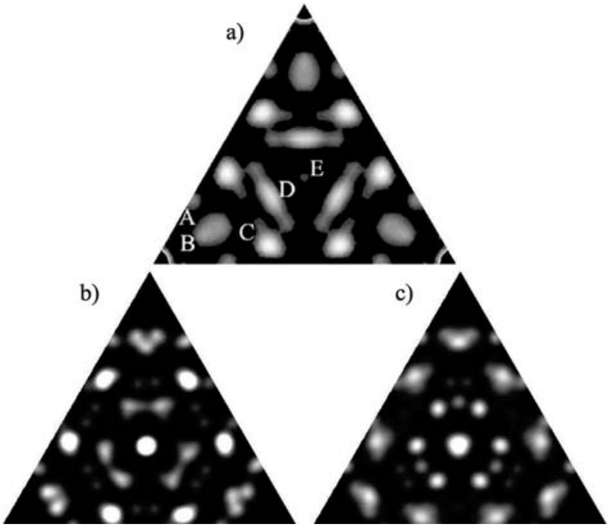

Figure 5. (a) Experimental Patterson map reproduced from Aoyamaa et al.[48] and Patterson maps calculated from our DFT simulations of (b) the uniform reconstruction (Starke model) and (c) a unit cell with a given chirality surrounded by a uniform reconstruction with the opposite chirality. The intensity scale is the same in (b) and (c).

The numbers of occurrences of the various classes of configuration observed among the 117 clearly identifiable molecular topographies are as follows: (AAAA), 7; (AAAB), 50; (ABAB), 27; (ABBA), 14; (AABB), 9; (ABBB),10; (BBBB), 0. The fact that the ABAB class is not predominant indicates that statistically the molecules are most of the time not located upon a homochiral area. This observation tends to show that the homochiral domains are small, certainly not bigger than ~20 nm. Moreover, as mentioned in the previous section, the DFT calculations showed that a completely random reconstruction is not favorable, so the domains are at least a few nanometers in size. Consequently, we can estimate the typical width of a domain as roughly 10 nm. This explains why chirality at the nanoscale has not been observed to date using standard far-field surface-science techniques, all of which are sensitive to an average value over a macroscopic area. Once again, this size value should depend on the experimental parameters during the surface preparation, notably the temperature. No chirality on the clean SiC(0001) 3 × 3 surface was observed using STM either, simply because the tunneling current flows through the pyramidal structures regardless of the position of the tip and thus does not probe directly the chiral Si adlayer. In Figure 1, we can indeed see that only the pyramids are visible, appearing as a hexagonal array of bright spots. Presumably, the reason why the adlayer structure is revealed by the H_2Pc molecules lying on the surface is that the molecules cover the gap between neighboring pyramid structures and thus act as an electronic bridge between the underlying adlayer and the STM tip.

Patterson Maps. Patterson maps extracted from XRD experiments[48] can be compared with a calculated map of the Starke model. As Figure 5 shows, there are small differences between the two. We shall see that the presence of contiguous left- and right-handed domains can explain some discrepancies. The Patterson map of a surface reconstruction is defined as the autocorrelation function of the electron density of the core electronic levels. Each spot defines a vector that represents one interatomic distance and orientation. Figure 5a displays the

---

(48) Aoyamaa, T.; Akimotoa, K.; Ichimiyaa, A.; Hisadab, Y.; Mukainakanob, S.; Emotoc, T.; Tajirid, H.; Takahashid, T.; Sugiyamae, H.; Zhange, X.; Kawatae, H. *Appl. Surf. Sci.* **2003**, *216*, 356.

experimental Patterson map extracted from the XRD measurements by Aoyamaa et al.[48] Figure 5b shows the Patterson map associated with the Starke model that we calculated from the DFT simulations. In order to match the experimental results, it is necessary to symmetrize the Patterson map by summing the Patterson maps associated with the right and left chiralities. As mentioned by Aoyamaa et al.,[48] there are two major discrepancies between the experimental Patterson map (Figure 5a) and the calculated map for the Starke model (Figure 5b): the central spot (E) is much brighter in the model than the experiment, and the bright, rod-like diffraction spot (D) in Figure 5a appears as only two separate spots in the Starke model. Figure 5c shows the calculated Patterson map for our chiral surface composed of a left-handed unit cell surrounded by uniform right-handed reconstruction (the choice is not important, as the opposite chirality is equivalent). To compare this calculated Patterson map with the experimental one, symmetrization must be done as before. The differences between the maps in Figure 5b,c are a consequence of the heterochirality: the boundaries between the right- and left-handed domains are characterized by atoms that are displaced compared with the uniform reconstruction. We can see that spot E has decreased in intensity and that spot D now has three components, corresponding to the three Si atoms at the base of the pyramid-like structures (the Si trimers; see Figure 3). When a local change in the chirality is performed in one unit cell, as in our simulations, some Si trimer atoms are translated slightly, as can be seen in Figures 3d and 4f. The effect on the Patterson map is the appearance of a new spot located between the two separated D spots of the homochiral reconstruction. Since this new spot is located between the two original D spots, this feature could explain fairly well the merging of spot D into a rod-like feature, as observed on the experimental map. Furthermore, in comparison with Figure 5b, the intensity of spot E in Figure 5c is reduced by 53%, which also tends toward the experiment. This latter feature is explained as follows. Each pyramid has three legs (Si trimers) which are linked to three adlayer domains, and each of them can display either right or left chirality. When the number of identical chiralities around the pyramid is not balanced (2:1), the pyramid is slightly shifted from the vertical position, which introduces a widening of spot E and thus a reduction of its maximum intensity. Li et al. have shown in a recent article[49] that Si adatoms missing at the top of the pyramids can lead to a weakening of peak E and a broadening of peak D in the Patterson map. This is in good agreement with the experimental results and can also contribute to explaining the experimental Patterson map.

Conclusion

We have shown that the SiC(0001) 3 × 3 reconstruction can be described in terms of contiguous coexisting domains with right and left chiralities randomly distributed at the nanoscale. Until now, no signature of this unusual translational symmetry breaking had ever been observed by any surface-science technique. Here, single hydrogenated phthalocyanine molecules act as molecular lenses to probe the underlying surface structure with subnanometer resolution. A heterochiral surface description resolves some of the principal discrepancies between the Starke model and XRD experiments. DFT calculations showed that the ground state corresponds to the homochiral 3 × 3 reconstruction while a heterochiral reconstruction is metastable. The energy change per unit length of the boundary between domains of different chiralities is evaluated to be 90 meV/Å. The principle of maximum entropy explains why the random heterochiral reconstruction is observed preferentially. Conversion to the homochiral ground state is prohibited at room temperature because a huge number of bonds would need to be broken.

Heterochirality should significantly affect the electronic surface transport of the SiC(0001) 3 × 3 reconstruction since the long-range periodicity is broken, enhancing electronic scattering. This could partly explain recent reports of very low electronic conductivity of the electronic surface states.[24] If an homochiral reconstruction could be obtained on the SiC(0001) 3 × 3 surface, this could pave the way for enantioselective biosensors and heterogeneous catalysis.

Acknowledgment. This work was supported by the ANR project MOLSIC (n° ANR-08-NANO-030) and the program C'Nano of the Région Ile de France. We thank the Institut du Développement et des Ressources en Informatique Scientifique (IDRIS) for allocation of computer time.

JA806002K

---

(49) Li, Y.; Ye, L.; Wand, X. *Surf. Sci.* **2006**, *600*, 298.